

Cite this: *Phys. Chem. Chem. Phys.*, 2011, **13**, 8560–8570

www.rsc.org/pccp

A crossed beam and *ab initio* investigation of the reaction of boron monoxide (^{11}BO ; $X^2\Sigma^+$) with acetylene (C_2H_2 ; $X^1\Sigma_g^+$)[†]

Dorian S. N. Parker,^a Fangtong Zhang,^a Pavlo Maksyutenko,^a Ralf. I. Kaiser^{*a} and Agnes H. H. Chang^b

Received 8th November 2010, Accepted 17th March 2011

DOI: 10.1039/c0cp02458a

The reaction dynamics of boron monoxide (BO ; $X^2\Sigma^+$) with acetylene (C_2H_2 ; $X^1\Sigma_g^+$) were investigated under single collision conditions at a collision energy of 13 kJ mol^{-1} employing the crossed molecular beam technique; electronic structure RRKM calculations were conducted to complement the experimental data. The reaction was found to have no entrance barrier and proceeded *via* indirect scattering dynamics initiated by an addition of the boron monoxide radical with its boron atom to the carbon–carbon triple bond forming the $\text{O}^{11}\text{BHCCH}$ intermediate. The latter decomposed *via* hydrogen atom emission to form the linear O^{11}BCCH product through a tight exit transition state. The experimentally observed sideways scattering suggests that the hydrogen atom leaves perpendicularly to the rotational plane of the decomposing complex and almost parallel to the total angular momentum vector. RRKM calculations indicate that a minor micro channel could involve a hydrogen migration in the initial collision to form an $\text{O}^{11}\text{BCCH}_2$ intermediate, which in turn can also emit atomic hydrogen. The overall reaction to form O^{11}BCCH plus atomic hydrogen from the separated reactants was determined to be exoergic by $62 \pm 8 \text{ kJ mol}^{-1}$. The reaction dynamics were also compared with the isoelectronic reaction of the cyano radical (CN ; $X^2\Sigma^+$) with acetylene (C_2H_2 ; $X^1\Sigma_g^+$) studied earlier.

1. Introduction

Currently the most widely used combustion processes in air-breathing rocket propulsion systems rely on the oxidation of carbon-bearing molecules.^{1,2} In the refinement of air-breathing, ramjet and scramjet rocket propulsion systems,³ which demand high energy per mole as well as high energy per volume and molecular weight, novel oxidation processes have been investigated, such as the oxidation of boron.^{4–6} The complete reaction of boron with molecular oxygen forms boron oxide (B_2O_3) which releases up to 630 kJ mol^{-1} ;⁷ this is three times greater than the energy release of the best hydrocarbon jet propellants (JP-10). Boron combustion was first studied by Russian scientists^{8–11} and was thought to be a potential breakthrough in solid state rocket fuels. The oxidation of boron is initially unable to reach full energy release⁴ due to the formation of boron oxide (B_2O_3), an inert layer which coats the non-reacted boron, preventing further reaction.^{12,13} This is unlike carbon combustion which forms carbon dioxide (CO_2) that rapidly migrates away from the

combustion zone. Boron combusts in two steps.^{13–16} The first is a weak glowing in which the oxide layer is removed through gasification, called the ignition stage. The second, the combustion phase, presents a vigorous burning of a heterogeneous type due to the high boiling point of boron (3900–4140 K). Currently, boron is utilized as pellets within conventional carbon based fuels. Essentially, the carbon-based fuel ignites and reaches a high enough temperature to remove the boron oxide layer, which, in turn, allows clean boron to be accessible for the combustion phase. This approach, however, is energetically costly, and a refinement of the process is highly desirable. This requires a detailed knowledge of the underlying elementary reactions in boron-doped combustion systems.

The mixture of carbon- and boron-based combustibles results in a complex combustion chemistry; the modeling of this system involves detailed experimental input parameters, such as reaction products and rate constants.^{17–21} Although the reaction dynamics of boron atoms with hydrocarbon molecules, such as acetylene (C_2H_2),^{22–24} ethylene (C_2H_4),^{25,26} benzene (C_6H_6),^{27,28} allene (C_3H_2),²⁹ dimethylacetylene ($\text{CH}_3\text{C}_2\text{CH}_3$)³⁰ and methylacetylene ($\text{CH}_3\text{C}_2\text{H}$),³¹ have emerged during recent years utilizing the crossed molecular beam approach, thus accessing the B/C/H system,³² surprisingly few kinetic and dynamics studies have been conducted on the B/O/C/H system. A variety of models have been developed to simulate the core parts of the combustion cycle based on the

^a Department of Chemistry, University of Hawaii at Manoa, Honolulu, HI

^b Department of Chemistry, National Dong Hwa University, Shoufeng, Hualien 974, Taiwan

[†] Electronic supplementary information (ESI) available. See DOI: 10.1039/c0cp02458a

rate of diffusion of oxygen and boron through the boron oxide layers. King developed an early model³³ with the diffusion rate of oxygen through the oxide layer as the rate determining step based on experiments by Macek *et al.*^{14,15} This model was refuted by Williams *et al.*^{34–36} and Kuo *et al.*^{37,38} who proposed a model with the diffusion of boron through the oxide layer as the rate determining step based on the experiments of Kuo *et al.*^{38,39} Nevertheless, the question over the dominant diffusion process has remained inconclusive. Zhou, Kolb, Rabitz *et al.* investigated a molecular level gas phase kinetic model for the homogenous chemistry of the B/O/H/C/F combustion system. The authors acknowledged that insufficient experimental data exist to complete this model. Information like the entrance barriers, rates of reactions, and products are lacking. A recent model^{40,41} derived from Kuo *et al.*'s³⁸ approach utilized generic global reactions in three stages: particle heating without reaction (ignition delay), first stage of combustion (oxide layer removal), and second stage of combustion (clean boron oxidation). Until now, the Zhou, Kolb, Rabitz *et al.*²¹ model remains the most comprehensive and it is utilized to investigate simpler models like those of Pfitzners *et al.*,^{40,41} highlighting the demand for experimentally determined input parameters.

A particular shortcoming is that the elementary reactions in the B/O system have never been coupled with those occurring in the B/C/H system. Most importantly, the oxidation of boron undertakes several stages involving the schematic reaction sequence $B \rightarrow BO \rightarrow BO_2 \rightarrow B_2O_3$.⁴² The formation of the doublet boron monoxide (BO; $X^2\Sigma^+$) radical presents the very first oxidation step. Considering its stability under combustion conditions, its reaction with combustion species such as hydrocarbon fuel presents an important class of reactions to be studied. Nevertheless, the reaction dynamics of boron monoxide (BO; $X^2\Sigma^+$) have been poorly investigated to date and have never been coupled with hydrocarbons. Only some experimental data exist. The kinetics of the reaction of boron monoxide with molecular oxygen has been reported by Nelson *et al.*⁴³ Under combustion conditions they found that the reaction proceeds through a bound BO_3 complex and lacks any pressure dependence. The rate constant was extrapolated to $7.7 \times 10^{-12} \text{ cm}^3 \text{ s}^{-1}$ in the formation of boron dioxide (BO_2) plus atomic oxygen. The energetics^{44,45} and kinetics⁴³ of the reaction of boron monoxide (BO) and molecular hydrogen (H_2) has been investigated as well due to the interest in the formation of gas-phase HOB and HBO molecules which have been deemed to withdraw considerable energy from the boron combustion process. The investigators⁴³ found the reaction to HBO to be exothermic with a $\Delta H = -250 \text{ kJ mol}^{-1}$, as predicted theoretically.³³ They also determined the rate constant, $k(T)$, to be $7.49 \times 10^{-23} \text{ cm}^3 \text{ s}^{-1} \text{ T}^{3.53} \exp(-1590/T)$ for a temperature range of 300–3000 K.

The reaction dynamics of the boron monoxide radical (BO; $X^2\Sigma^+$) with unsaturated hydrocarbons has not been investigated either experimentally or theoretically to date. Therefore, we have initiated a systematic research program to elucidate the reaction dynamics of boron monoxide with unsaturated hydrocarbon molecules under single collision conditions as provided in crossed molecular beam experiments. This work presents data on the bimolecular gas phase

reaction of ground state boron monoxide with acetylene (C_2H_2 ; $X^1\Sigma_g^+$) as the simplest alkyne. Since limited theoretical data⁴⁶ on the system is available, we also explore the reaction computationally. Note that besides the interest from the chemical dynamics viewpoint and from the combustion communities, the boron monoxide radical (BO; $X^2\Sigma^+$) is also of interest to the physical organic and physical inorganic communities as it is isoelectronic to the cyano radical (CN; $X^2\Sigma^+$).^{46–49} The effect on vertical and electron detachment energies of boronyl substituted acetylene was recently investigated using DFT calculations.⁴⁶ Here, the system was compared to similar cyano substituted hydrocarbons and it was found that the boronyl group serves as a sigma-radical in these covalent systems similar to the cyano group in cyano substituted hydrocarbons and hydrogen in hydrocarbons. Boron monoxide has an ionization energy of 13.3 eV, only 0.2 eV less than the cyano radical. The isoelectronic characteristics are also reflected in their $^2\Sigma^+$ electronic ground state. Their respective heat capacities are $29.20 \text{ J K}^{-1} \text{ mol}^{-1}$ and $29.16 \text{ J K}^{-1} \text{ mol}^{-1}$; also, their bond strengths are on the same order of magnitude, for BO, 806 kJ mol^{-1} , and CN, 770 kJ mol^{-1} , along with their internuclear distances of 1.205 \AA and 1.172 \AA , respectively. The shorter carbon–nitrogen bond can be visualized as a carbon–nitrogen triple bond, whereas boron monoxide holds a boron–oxygen double bond. The distinct bond orders are also reflected in the lower vibrational frequency of boron monoxide of 1885 cm^{-1} versus 2068 cm^{-1} for the cyano radical. The bond distances result in rotational constants, B , of 1.7811 cm^{-1} and 1.89974 cm^{-1} for boron monoxide and the cyano radical, respectively. Therefore, due to the isoelectronic character of the boron monoxide and the cyano radical, the reaction dynamics and potential energy surface of the $BO-C_2H_2$ system will also be compared with the isoelectronic $CN-C_2H_2$ system studied previously in our group.⁵⁰

2. Experimental and data analysis

The experiments were carried out under single collision conditions in a crossed molecular beams machine at the University of Hawaii.⁵¹ Briefly, a supersonic beam of ground state boron monoxide (BO; $X^2\Sigma^+$) was produced *in situ via* laser ablation of boron utilizing a pulsed carbon dioxide beam (CO_2 , 99.9999%, BOC gases)⁵² in the primary source region of the vacuum chamber. The boron was ablated by focusing the 4th harmonic of a Spectra-Physics Quanta-Ray Pro 270 Nd:YAG laser operating at 1064 nm and 30 Hz onto the rod at a peak power of 7–9 mJ per pulse. The rotating boron rod was mounted on a home-made ablation source.⁵² The carbon dioxide (CO_2 ; $X^1\Sigma_g^+$) carrier gas was introduced *via* a Proch-Trickl pulsed valve, operating at repetition rates of 60 Hz with amplitudes of -400 V and opening times of 80 μs , where it reacted with the ablated boron (B ; 2P_1) atoms to produce boron monoxide (BO; $X^2\Sigma^+$). A backing pressure of 4 atm for the carbon dioxide (CO_2 ; $X^1\Sigma_g^+$) source was used resulting in a pressure of $4 \times 10^{-4} \text{ Torr}$ in the primary source. The molecular beam including the boron monoxide (BO; $X^2\Sigma^+$) passed a skimmer and a four-slot chopper wheel, which selected a segment of the pulsed boron monoxide (BO; $X^2\Sigma^+$) beam of a well-defined peak velocity (v_p) and speed ratio (S).

Table 1 Peak velocities (v_p), speed ratio (S), and the center-of-mass angles (Θ_{CM}), together with the nominal collision energies (E_{col}) of acetylene and boron oxide molecular beams

	v_p (ms ⁻¹)	S	E_{col} (kJ mol ⁻¹)	Θ_{CM}
C ₂ H ₂	900 ± 10	9.0 ± 0.2	13.0 ± 0.8	38.3 ± 1.2
BO	1162 ± 12	3.0 ± 0.3		

The primary beam characteristics were $v_p = 1162 \pm 12$ ms⁻¹ and $S = 3.0 \pm 0.3$ (Table 1). The boron monoxide (BO; $X^2\Sigma^+$) beam bisected a pulsed beam of acetylene (C₂H₂; $X^1\Sigma_g^+$) at 90° (C₂H₂, 99.9% purity after removal of acetone *via* zeolite traps and an ethanol-dry ice bath) released by a second pulsed valve at 550 Torr with a peak velocity $v_p = 900 \pm 10$ ms⁻¹ and speed ratio of 9.0 ± 0.2 (Table 1). The secondary pulsed valve was operated at repetition rates of 60 Hz, amplitudes of -500 V and opening times of 80 μs. Assisted by two frequency dividers (Pulse Research Lab, PRL-220A) and three pulse generators (Stanford Research System, DG535), a photodiode mounted on top of the chopper wheel provided the time zero trigger for the experiment. The primary and secondary pulsed valves opened 1840 μs and 1882 μs after the time zero as defined by the photo diode. The relative timings for the experiment are illustrated in Fig. 1. The collision energy between the boron monoxide (BO; $X^2\Sigma^+$) and acetylene (C₂H₂; $X^1\Sigma_g^+$) molecules was 13.0 ± 0.8 kJ mol⁻¹. Boron has two isotopes, $m/z = 11$ (80%) and $m/z = 10$ (20%), of which the reported collision energy refer to the ¹¹B(²P_j) isotope. In principle, the reaction of the boron atom (¹¹B; ²P_j) with carbon dioxide (CO₂; $X^1\Sigma_g^+$) in the ablation center can also give products other than boron monoxide (¹¹BO; $X^2\Sigma^+$). Therefore, a wide range of potential co-reactants were carefully tested for the empiric formulas C_xB_yO_z ($x = 0, 1, y = 0-5, z = 0-4$). The only background peaks were found at $m/z = 55$ and $m/z = 54$ at levels of a few percent, which correspond to either ¹¹B₅/¹⁰B¹¹B₄ clusters or formation of diboron dioxide (¹¹B₂O₂).

The reaction products were monitored using a triply differentially pumped quadrupole mass spectrometer (QMS) in the time-of-flight (TOF) mode after electron-impact ionization of the neutral molecules at 80 eV with an emission current of 2 mA. These charged particles were separated according to their mass-to-charge ratio by an Extrel QC 150 quadrupole mass spectrometer operated with an oscillator at 2.1 MHz; only ions with the desired mass-to-charge, m/z , value passed through and were accelerated toward a stainless steel 'door knob' target coated with an aluminium layer and operated at a voltage of -22.5 kV. The ions hit the surface and initiated an electron cascade that was accelerated by the same potential until they reached an aluminium coated organic scintillator, whose photon cascade was detected by a photomultiplier tube (PMT, Burle, Model 8850, operated at -1.35 kV). The signal from the PMT was then filtered by a discriminator (Advanced Research Instruments, Model F-100TD, level: 1.4 mV) prior to feeding into a Stanford Research System SR430 multichannel scaler to record time-of-flight spectra.^{53,54} TOF spectra were recorded at 2.5° intervals over the angular distribution with 2.6×10^5 TOF spectra recorded at each angle.

The TOF spectra recorded at each angle and the product angular distribution in the laboratory frame (LAB) were fitted with Legendre polynomials using a forward-convolution routine.^{55,56} This method uses an initial choice of the product translational energy $P(E_T)$ and the angular distribution $T(\theta)$ in the center-of-mass reference frame (CM) to create TOF spectra and a product angular distribution. The TOF spectra and product angular distribution obtained from the fit were then compared to the experimental data. The parameters $P(E_T)$ and $T(\theta)$ were iteratively optimized until the best fit was reached. The parameters found were then used to create a visually intuitive representation of the chemical dynamics in the form of a contour plot. Here, the product flux contour map, $I(\theta, u) = P(u) \times T(\theta)$, is a plot of the intensity of the reactively scattered products (I) as a function of the CM

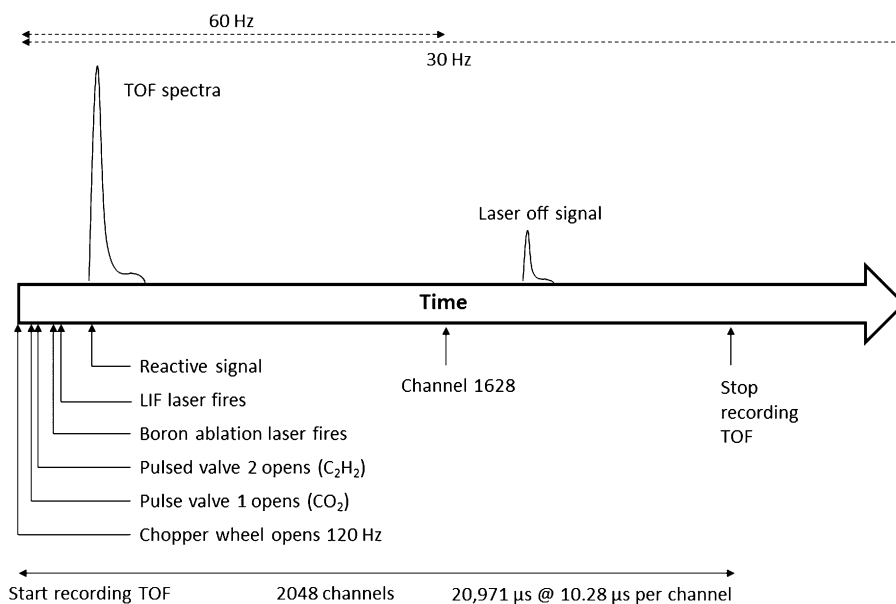


Fig. 1 Timeline for the crossed molecular beam experiment of boron monoxide radicals (¹¹BO; $X^2\Sigma^+$) with acetylene (C₂H₂; $X^1\Sigma_g^+$), and the laser induced fluorescence (LIF) laser.

scattering angle (θ) and product velocity (u). This plot is the reactive *differential cross section* and gives an *image* of the chemical reaction. Processing of the raw TOF spectra to averaged TOF spectra and the product angular distribution was conducted using a newly written Labview program code. This program normalizes the TOF data based on the data accumulation times and drifts in the intensity of the carbon beam.

For polyatomic radicals, it is also important to characterize the rovibrational states. Here, we utilized laser induced fluorescence (LIF) to extract the rotational and vibrational temperature of the boron monoxide (BO; $X^2\Sigma^+$) beam segment which crossed the acetylene beam (C_2H_2 ; $X^1\Sigma_g^+$). Our *in situ* LIF detection setup has been described recently.⁵⁷ The ground state of boron monoxide was probed *via* the $A^2\Pi-X^2\Sigma^+$ (0,0) transition at ~ 425 nm by the pulsed 10 μ J output of a Lambda Physik Scanmate dye laser pumped by the third harmonic of an integrated Nd:YAG laser operating at 10 Hz with an output power of 50 mJ per pulse. The dye laser was delayed relative to the pulsed valve opening time to intercept the peak of the boron monoxide beam. The timing of the LIF relative to the experiment is integrated in Fig. 1. The fluorescence was detected by a Hamamatsu R955 photomultiplier tube (PMT) filtered by a Schott color glass long-pass GG-495 filter for (2,0) fluorescence detection and scattered detection laser light suppression. The signal was then amplified by a built-in amplifier of the Hamamatsu C7247 PMT socket assembly and filtered by a high pass filter prior to feeding into a digital oscilloscope interfaced to a computer for data collecting and processing. The LIF spectra were then analyzed utilizing the diatomic spectral simulation program by Tan.⁵⁸ We adopted spectroscopic constants for the $A^2\Pi-X^2\Sigma^+$ system from Melen *et al.*⁵⁹ Note that boron monoxide radicals are expected to be exclusively in the ground electronic state, $X^2\Sigma^+$, by the time they reach the interaction region. The radiative lifetime⁶⁰ of the first excited electronic state, $A^2\Pi_{\pm 1/2}$, of boron monoxide of 1.8 μ s is shorter than the 50 μ s flight time from the ablation region to intersection point.

3. Theoretical methods

Probable reaction paths in the reaction of BO($X^2\Sigma^+$) with $C_2H_2(X^1\Sigma_g^+)$ are explored by *ab initio* electronic structure calculations. The intermediates, transition states, and dissociation products are characterized such that their optimized geometries and harmonic frequencies are obtained at the level of the hybrid density functional theory, the unrestricted B3LYP^{61,62}/cc-pVTZ, and the energies are refined with the coupled cluster^{63–66} CCSD(T)/cc-pVTZ with B3LYP/cc-pVTZ zero-point energy corrections, if not otherwise stated. The barrierless formation of the collision complex **11** is confirmed by intrinsic reaction coordinates calculations (IRC) at the unrestricted B3LYP/cc-pVTZ level of theory along the C–B bond distance. The GAUSSIAN 03 programs⁶⁷ are utilized in the electronic structure calculations.

Assuming the energy is equilibrated among molecular degrees of freedom before the reaction occurs, and provided the energy is conserved such as in molecular beam experiments, the rate constant could be predicted by RRKM theory.

For a reaction $A^* \xrightarrow{k} A^\ddagger \rightarrow P$, where A^* is the energized reactant, A^\ddagger represents the transition state, and P the products, the rate constant $k(E)$ may be expressed as

$$k(E) = \frac{\sigma W^\ddagger (E - E^\ddagger)}{h \rho(E)} \quad (1)$$

where σ is the symmetry factor, W^\ddagger the number of states of the transition state, E^\ddagger the transition state energy, and ρ the density of states of the reactant. ρ and W^\ddagger are computed by saddle-point method, molecules are treated as collections of harmonic oscillators whose harmonic frequencies are obtained by B3LYP/cc-pVTZ as described above.⁶⁸

4. Results

4.1 Experimental results

The reactive scattering signal was recorded at mass-to-charge ratios, m/z , of 52 ($^{11}\text{BOC}_2\text{H}^+$), 51 ($^{11}\text{BOC}_2^+ / ^{10}\text{BOC}_2\text{H}^+$), and 50 ($^{10}\text{BOC}_2^+$). The TOF spectra at $m/z = 50$ and 51 had—after scaling—the same profile compared to those recorded at $m/z = 52$. These observations alone suggest that signal at lower masses originated from dissociative ionization of the parent ion and/or from reaction of the (^{10}BO ; $X^2\Sigma^+$) reactant with acetylene (C_2H_2 ; $X^1\Sigma_g^+$). Further, only the hydrogen atom loss channel is open in this mass range; the molecular hydrogen loss channel is closed. Fig. 2 depicts selected TOF spectra recorded at $m/z = 52$ ($^{11}\text{BOC}_2\text{H}^+$). It should be noted that the fits of the TOF spectra were conducted using a single channel with a mass combination of 52 amu ($^{11}\text{BOC}_2\text{H}^+$) and 1 amu (H). The TOF spectrum at each angle was integrated and scaled by the number of scans taken and beam intensities to derive the laboratory angular distribution (LAB) of the $^{11}\text{BOC}_2\text{H}$ products at the most intense m/z value of 52 ($^{11}\text{BOC}_2\text{H}^+$) (Fig. 3). The laboratory angular distribution extends by at least 45° in the scattering plane defined by the primary and secondary beams. The center-of-mass (CM) angle of $38.3^\circ \pm 1.2^\circ$ is indicated in

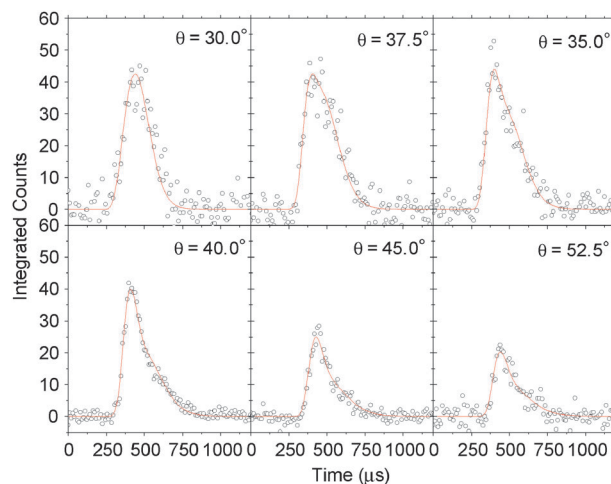


Fig. 2 Time-of-flight data at various angles recorded at $m/z = 52$ for the reaction of boron monoxide (^{11}BO ; $X^2\Sigma^+$) with acetylene (C_2H_2 ; $X^1\Sigma_g^+$) at a collision energy of 13.0 ± 0.8 kJ mol⁻¹. The circles indicate the experimental data, and the solid lines indicate the calculated fit.

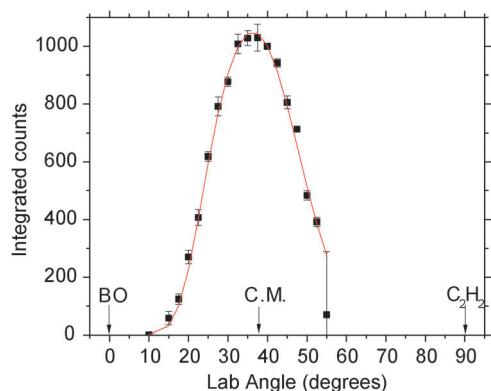


Fig. 3 Laboratory angular distribution (LAB) of the $^{11}\text{BOC}_2\text{H}$ isomer(s), $m/z = 52$, formed in the reaction of boron monoxide (^{11}BO ; $\chi^2\Sigma^+$) with acetylene (C_2H_2 ; $\chi^1\Sigma_g^+$) at a collision energy of $13.0 \pm 0.8 \text{ kJ mol}^{-1}$. Circles and error bars indicate experimental data, and the solid line indicates the calculated distribution.

Fig. 3, while the fit peaks at $37.5^\circ \pm 0.5^\circ$; this observation suggests that the reaction proceeds *via* indirect (complex forming) scattering dynamics involving $^{11}\text{BOC}_2\text{H}_2$ reaction intermediate(s).

By using the fits of the forward convolution fitting routine to the laboratory data we obtain information on the chemical dynamics of the system. The CM translational energy distribution (Fig. 4 (top)), $P(E_T)$, as derived from the best fits with a single channel, shows a maximum translational energy release of $75 \pm 8 \text{ kJ mol}^{-1}$. From the conservation of energy law we can calculate the reaction exoergicity by subtracting the collision energy from the maximum energy released. Here, we see the reaction forming $^{11}\text{BOC}_2\text{H}$ isomer(s) plus atomic hydrogen to be exoergic by $62 \pm 8 \text{ kJ mol}^{-1}$. Also, as can be seen from the $P(E_T)$, the flux distribution peaks away from zero translational energy at about 25 to 30 kJ mol^{-1} . This indicates that at least one reaction channel to form the $^{11}\text{BOC}_2\text{H}$ isomer(s) has a tight exit transition state (repulsive bond rupture involving a significant electron rearrangement). The CM translational energy distribution $P(E_T)$ also allows us to determine the amount of energy released into the translational degrees of freedom of the products to be $35 \pm 5 \text{ kJ mol}^{-1}$ (about 45% of the total available internal energy).

The CM angular distribution, $T(\theta)$, is shown in Fig. 4 (bottom) and possesses a number of important features. Firstly, the distribution shows intensity over the whole angular range which is indicative of an indirect, complex-forming reaction mechanism. Secondly, the CM angular distribution is forward scattered in the direction of the boron monoxide beam ($\theta = 0^\circ$) with a ratio of intensities at the poles, $I(180^\circ)/I(0^\circ)$, of 0.71 ± 0.12 . This feature shows that the lifetime of the complex is about a fraction of 0.69 of its rotational period, in line with the osculating complex model⁶⁹ of the chemical reaction. Lastly, the CM angular distribution depicts a peak at $\theta = 80^\circ$ suggesting geometrical constraints when the decomposing complex emits a hydrogen atom. The peak shape indicates a preferential hydrogen loss parallel to the total angular momentum vector. The above characteristics can be seen in the flux contour map (Fig. 5). The flux distribution shows a peaking in the forward direction as well

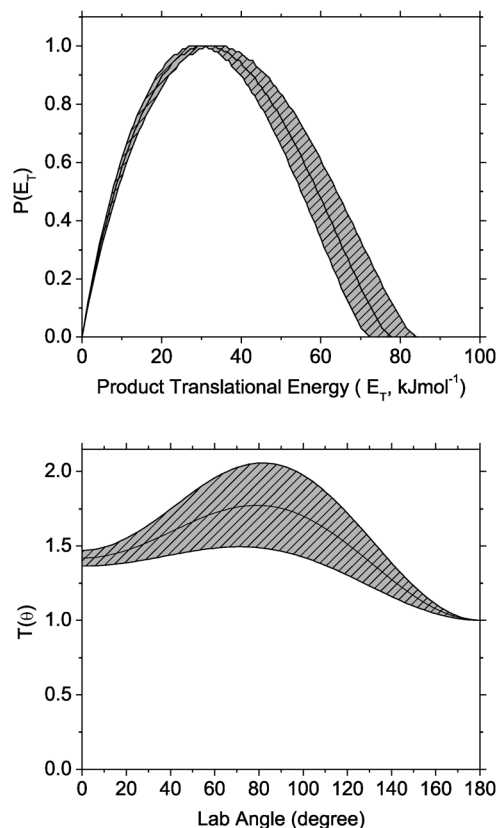


Fig. 4 Center-of-mass translational energy distribution (top) and center-of-mass angular distribution (bottom) for the reaction of boron monoxide (^{11}BO ; $\chi^2\Sigma^+$) with acetylene (C_2H_2 ; $\chi^1\Sigma_g^+$) to form $^{11}\text{BOC}_2\text{H}$ radical(s) and atomic hydrogen at a collision energy of $13.0 \pm 0.8 \text{ kJ mol}^{-1}$. The shaded area represents a 10% increase in the sum of chi squared for all fits to the TOF data when altering fitting parameters relating to the product translational energy and COM angular distribution, respectively.

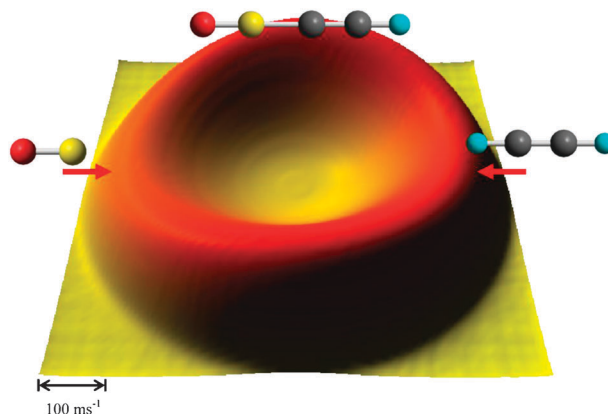


Fig. 5 Flux contour map of the reaction of boron monoxide (^{11}BO ; $\chi^2\Sigma^+$) with acetylene (C_2H_2 ; $\chi^1\Sigma_g^+$) to form $^{11}\text{BOC}_2\text{H}$ radical(s) and atomic hydrogen at a collision energy of $13.0 \pm 0.8 \text{ kJ mol}^{-1}$.

as a sideways-scattering pattern. It should be noted that the laboratory angular distribution (LAB) and time of flight spectra could not be fit with an isotropic distribution.

The excitation LIF spectrum utilizing $A^2\Pi_r-\chi^2\Sigma^+$ transitions (Fig. 6) allows us to probe rovibrational state populations in

structure calculations predict that the hydrogen atom exits at an angle of 80.9° with respect to the principal rotation axis (Fig. 9). The second reaction pathway leads from **i1** to **i3** ($\text{O}^{11}\text{BCCH}_2$) *via* a hydrogen migration to the terminal carbon; this pathway has a large energy barrier of 174 kJ mol^{-1} . From **i3**, **p1** can then be reached *via* a hydrogen loss from the terminal carbon with subsequent electron rearrangement by overcoming a tight exit transition state located 17 kJ mol^{-1} above the separated products. Here, the hydrogen loss is predicted to occur at an angle of 101.7° with respect to the principal rotation axis (Fig. 9). Both of the reaction pathways lead to **p1**, the $\text{O}^{11}\text{BC}_2\text{H}$ product; the **i1-p1** pathway has an energy barrier 22 kJ mol^{-1} lower than the **i3-p1** pathway, so it should be preferential. This is reflected in the results of our RRKM calculations. The pathway from **i1/i2** to **p1** plus atomic hydrogen is clearly dominant with an overall percentage of reaction of 96.3% while the reaction involving **i3** is minor with fractions of 3.7% at the collision energy of 13 kJ mol^{-1} . This fraction varies very little with the collision energy from 0.0 kJ mol^{-1} to 41.8 kJ mol^{-1} from 1.1% to 6.2%.

Having discussed the pathways which are accessible under our experimental conditions, we will focus for completeness on the remaining stationary points of the $^{11}\text{BOC}_2\text{H}_2$ potential energy surface. Intermediate **i2** can form in principle a cyclic intermediate **i5** by passing a barrier of 258 kJ mol^{-1} . However, the barrier is higher than the collision energy, and therefore, this intermediate cannot be accessed under our experimental conditions. This situation holds also for intermediates **i7** and **i8**. The intermediate **i8** is also accessible from the reactants (*via* a barrier of 160 kJ mol^{-1}). After a hydrogen migration from **i8** to the terminal carbon atom *via* an energy barrier of 195 kJ mol^{-1} , **i9** with an energy of 89 kJ mol^{-1} is formed. This structure can also be reached *via **i6**, which in turn is formed from **i3**: firstly **i6**, with an energy of 11 kJ mol^{-1} , is accessed from **i3** by a barrier of 130 kJ mol^{-1} . Formally, intermediates **i7–i9** are related to **i1–i3** by adding to the carbon–carbon triple bond *via* the oxygen atom of the boron monoxide radical (**i7–i9**) as compared to the boron atom (**i1–i3**). The reactants can form the products **p2** ($\text{HBO} + \text{C}_2\text{H}$) at a relative energy of 90 kJ mol^{-1} by overcoming an energy barrier of 106 kJ mol^{-1} and the products **p3** ($\text{BOH} + \text{C}_2\text{H}$) at a relative energy of 272 kJ mol^{-1} . The formation of **p4** ($\text{HC}_2\text{O}^{11}\text{B} + \text{H}$), a structure with the oxygen bonded to the acetylene group *via* a hydrogen loss, is endothermic by 289 kJ mol^{-1} . A product minimum **p5** ($\text{HCCB}^{11}\text{O} + \text{H}$) was found at 266 kJ mol^{-1} corresponding to a tetracyclic ring structure accessible from **i5** by overcoming a barrier of 286 kJ mol^{-1} . Finally, **p6** ($\text{CCHB}^{11}\text{O} + \text{H}$), a structure with boron bonded to carbon which is bonded to a hydrogen and the other carbon atom, has an energy of 133 kJ mol^{-1} . Since the energy of **i5–i9**, the transition states leading to these intermediates, and the products **p2–p6** are higher than the collision energy in our experiments, these intermediates cannot be accessed under our experimental conditions. The list of OBCCH isomers investigated is listed in the supplementary information.†*

5. Discussion

In order to elucidate the reaction pathway between boron monoxide and acetylene, we combined cross molecular beams

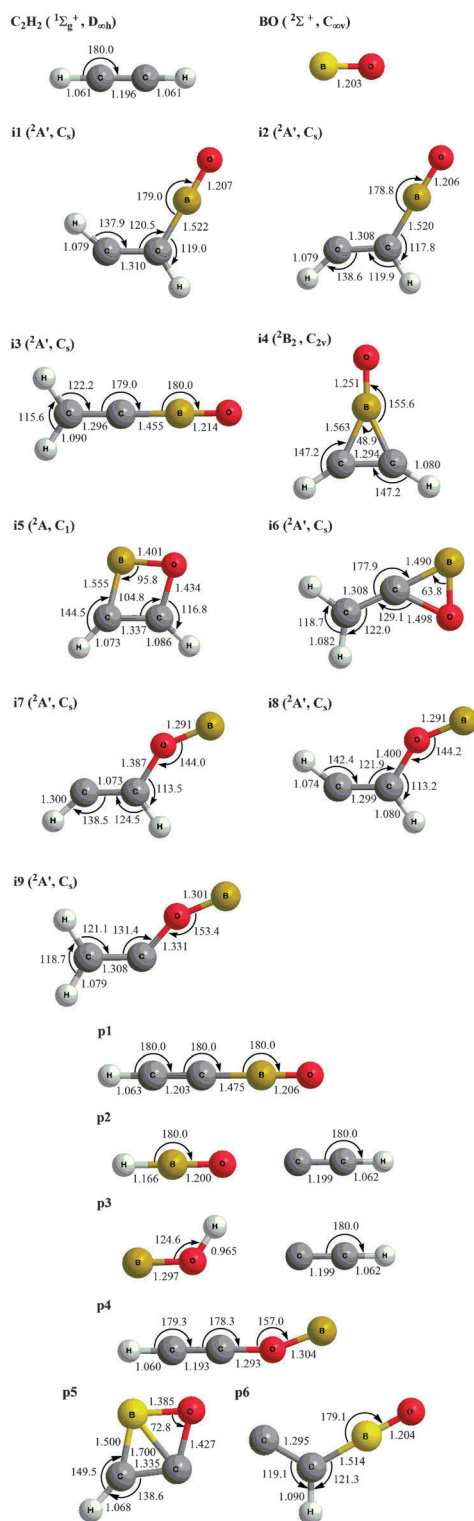


Fig. 8 Bond distances in angstroms and bond angles in degrees of intermediates, reactants, and products of the BOC_2H_2 potential energy surface.

experiments at a collision energy of $13 \pm 0.8 \text{ kJ mol}^{-1}$ with electronic structure calculations of the $\text{O}^{11}\text{BC}_2\text{H}_2$ potential energy surface. Firstly, let us compile the experimental results:

- The TOFs recorded at $m/z = 52$ are indicative of a product with an empiric formula of $\text{O}^{11}\text{BC}_2\text{H}^+$ and suggests

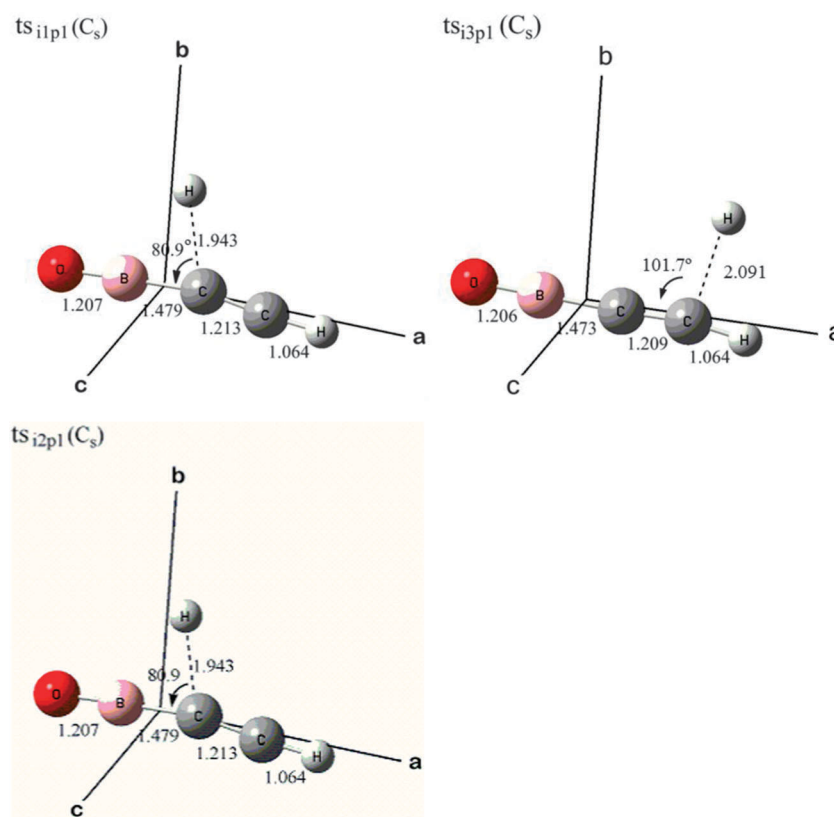


Fig. 9 Transition state geometries of hydrogen loss step to products for **i1-p1**, **i2-p1** and **i3-p1** pathways. Bond angle are given in degrees relative to principal rotation axis.

the reaction proceeds through a ^{11}BO versus hydrogen atom exchange pathway. No molecular hydrogen loss is present.

- The CM angular distribution, $T(\theta)$, shows intensity over the whole angular range in the reaction to form $\text{O}^{11}\text{BC}_2\text{H}$ isomers, showing the reaction proceeds *via* indirect scattering dynamics involving $\text{O}^{11}\text{BC}_2\text{H}_2$ collision complexes.

- The CM translational energy distribution $P(E_T)$, shows a reaction exoergicity of $62 \pm 8 \text{ kJ mol}^{-1}$, and peaks away from zero at 25–30 kJ mol^{-1} suggesting a tight exit transition state upon decomposition of the $\text{O}^{11}\text{BC}_2\text{H}_2$ intermediate to $\text{O}^{11}\text{BC}_2\text{H}$.

- The CM angular distributions, $T(\theta)$, is slightly forward scattered indicating the complex lifetime is shorter than the rotational period of the complex.

- The CM angular distribution depicts a distribution maximum centered at $\theta = 80^\circ$ suggesting the decomposing complex has a preferential hydrogen loss direction almost parallel to the total angular momentum vector.

Having summarized the experimental results we can identify first the product formed in the reaction of ^{11}BO with acetylene. The exoergicity of the ^{11}BO with acetylene reaction to form $\text{O}^{11}\text{BC}_2\text{H}$ was determined theoretically as 58 kJ mol^{-1} . The experimentally determined exoergicity of $62 \pm 8 \text{ kJ mol}^{-1}$ supports the synthesis of **p1** $\text{O}^{11}\text{BC}_2\text{H}$ plus atomic hydrogen and is well within the error boundaries of the experiment. It should be noted the next closest structural isomer **p4** is $\text{BO}^{11}\text{C}_2\text{H}$ which is endothermic by 289 kJ mol^{-1} relative to the reactants, so can be ruled out for the collision energy of

13 kJ mol^{-1} for this experiment. The LIF study shows ^{11}BO has been efficiently cooled by the supersonic expansion and only has a maximum of $2.0 \pm 0.3 \text{ kJ mol}^{-1}$ of internal energy. If we consider that acetylene is also efficiently cooled by the supersonic expansion we can subtract the maximum internal energy from the reaction exoergicity to obtain a value of the reaction of $60 \pm 8 \text{ kJ mol}^{-1}$ even closer to the theoretically determined value.

Since we have identified the product to be exclusively $\text{O}^{11}\text{BC}_2\text{H}$ plus atomic hydrogen, we can consider the reaction pathway to the product. A comparison of the structures of the reactants with the $\text{O}^{11}\text{BC}_2\text{H}$ suggests that the hydrogen atom in acetylene is replaced by the ^{11}BO group. Therefore, we propose that the ^{11}BO radical adds first to the carbon atom of the acetylene molecule forming intermediates **i1/i2**. Recall that the indirect nature of the reaction was verified experimentally based on the center-of-mass angular distribution. Both intermediates can decompose *via* hydrogen atom loss through tight transition states forming the $\text{O}^{11}\text{BC}_2\text{H}$ products. The reversed reaction, *i.e.* the reaction of a hydrogen atom with a closed shell molecule in which the hydrogen atom is adding to the carbon-carbon triple bond, is expected to have an entrance barrier. This principle of microscopic reversibility is clearly evident from the experimental and theoretical results. Besides the fragmentation of **i1/i2** to the products, note that the calculations predict, to a minor amount, the isomerization of **i1** to **i3**. The RRKM calculations show this pathway to be a minor channel of only a few percent. These results

reinforce the notion that the **i1/i2-p1** pathway is the major reaction route.

Is this reaction sequence also reflected in the shape of the center-of-mass angular distribution? The peaking of the CM angular distribution is indicative of a preferential hydrogen loss direction parallel to the total angular momentum vector; this argument can be used to rationalize the reaction pathway to the products. Let us consider the two intermediate structures that are able to form in the reaction to be $O^{11}BHCCH$ **i1/i2** and $O^{11}BCCH_2$ (**i3**) from which the hydrogen loss occurs, leading to the linear final product $O^{11}BCCH$ (**p1**). The H atom loss can either be from the primary carbon (**i1/i2**) or from the secondary carbon (**i3**) *via* H atom migration, an analogous scenario to the isoelectronic reaction of $CN + C_2H_2$.⁵⁰ Grice and Smith⁷⁰ used microcanonical theory to understand a similar problem for the reaction $OH + CO \rightarrow CO_2 + H$, which passes through a bent intermediate. Here, the authors approximated that β , the angle between the exiting hydrogen atom and the primary rotation axis, A, was 45° and found this to produce a broad peaked distribution, theoretically and experimentally. They also calculated that with $\beta = 90^\circ$, for a prolate linear rotor, the angular distribution would be heavily peaked. The current investigation fits into the same premises for the model, that the exiting species is a light hydrogen atom with an associated exit barrier, and the intermediate can be considered as a linear rotor. The differentiation between the intermediates $O^{11}BCCH_2$ (**i3**) and $O^{11}BHCCH$ (**i1/i2**) can be made by considering what distribution the hydrogen atom loss will produce from their differing locations. For the intermediate $O^{11}BCCH_2$ (**i3**), the exiting hydrogen atom comes from the terminal carbon that has another hydrogen atom attached to it; the equilibrium angle for β is 101.7° as shown in Fig. 9. The intermediate $O^{11}BHCCH$ (**i1/i2**) will result in the majority of the distribution closer to $\theta = 90^\circ$, since the hydrogen loss direction is perpendicular to the heavy carbon chain and principal rotation axis at $\beta = 80.9^\circ$ (Fig. 9). It is unlikely β will vary much due to the rigidity of the heavy carbon backbone and so will generate a peaked distribution. We can deduce that hydrogen loss from the $O^{11}BHCCH$ intermediate **i1/i2** is responsible for the heavily peaked distribution. These results indicate the intermediate **i3** is either not being accessed or if so in minimal quantities in this scheme. As a result of this mechanism the product will be excited to B-like rotations.

Let us now compare the present reaction of ^{11}BO with acetylene to the reaction of the cyano radical (CN) with acetylene—the isoelectronic system studied earlier in our group.⁵⁰ Both reactions follow indirect reactive scattering dynamics and about 33%–46% of the total available energy channels into translational degrees of freedom. Further, both CM angular distributions are forward scattered by approximately the same amount if scaled by the collision energy and diatomic rotational constants, indicating similar complex lifetimes. The reactions proceed by an attack of the diatomic radical center (the carbon atom in the CN reaction) onto the π_x/π_y electron density of the triple bond of acetylene *via* a loose transition state. Both surfaces have a similar *cis/trans* isomeric double potential well as their first barrier-less reaction intermediate, interchangeable by a small energy barrier;

for the cyano reaction the initial intermediate is 58 kJ mol^{-1} lower in relative energy terms. The linear cyanoacetylene (HCCCN) product can be reached from the initial intermediate by overcoming a barrier of 170 kJ mol^{-1} which is 30 kJ mol^{-1} higher than for the ^{11}BO reaction. In the CN reaction, this route to the products is the major reaction channel and is responsible for the peaking in the CM angular distribution due to the preferential hydrogen loss direction as is the case for the ^{11}BO reaction discussed above. The second micro channel to the linear product for both systems is reached from the global potential minimum which is -288 kJ mol^{-1} for the cyano reaction; 50 kJ mol^{-1} lower than the corresponding ^{11}BO intermediate. For the global potential minima, both have a structure with two terminal hydrogen atoms that is accessed from the initial intermediate by high energy barriers of $\sim 175 \text{ kJ mol}^{-1}$ associated with a hydrogen migration. This route is the minor reaction channel; the branching ratio between the major and minor reaction channels is 85:15 for the cyano radical reaction; for ^{11}BO it is 97:3. The larger percentage of the major reaction pathway in the BO reaction manifests itself as a more pronounced peak in the CM angular distribution compared with the CN reaction. The products for both systems have linear structures and are accessed by tight transition states of similar energies relative to the products, although the cyano reaction product is a third more exoergic. The cyano reaction is also able to proceed through an attack of the nitrogen on the acetylene molecule to reach an intermediate of -148 kJ mol^{-1} , whereas an attack by the oxygen atom of ^{11}BO is energetically inaccessible due to the higher barrier of 160 kJ mol^{-1} . A cyclic intermediate is also accessible as a primary reaction step; both surfaces have a similar relative energy for this structure. Also, the tetracyclic ring formation for the CN reaction is endothermic by 7 kJ mol^{-1} and is accessible from the primary intermediate by an energy barrier 10 kJ mol^{-1} greater than for the ^{11}BO system. In summary, the BO-acetylene and CN-acetylene potential energy surfaces have common features, and the reaction dynamics are similar, proceeding both indirectly *via* addition of the radical center to the carbon–carbon triple bond forming *cis/trans* HCCHX (X = CN, BO) radicals followed by atomic hydrogen loss. To a minor amount, the intermediate can undergo hydrogen shifts to form H_2CCX intermediate followed by hydrogen atom loss. In both cases, the hydrogen loss from the initial reaction intermediate dominates. Unlike the case of the CN-acetylene system, where the radical reactant can add both with its nitrogen or carbon atom to the acetylene, in the case of the BO reaction, *only* the addition *via* the boron atom has no entrance barrier. Therefore, at low temperatures, we expect that the reaction of CN with acetylene is faster by a factor of about two compared to the BO-acetylene system, simply because 50% of the collisions—those where the O atom of the BO reactants wants to add to the acetylene molecule—do not lead to reaction. This is similar to the reaction of the D1-ethynyl radical with acetylene studied earlier in our laboratory.⁷¹ Here, only the acetylenic radical center of the ethynyl radical could add to the carbon–carbon triple bond of acetylene, whereas the addition of the ethynyl radical *via* its HC-group involved a significant energy barrier; also, the low temperature rate constants of the ethynyl–acetylene reaction

were found to be a factor of about two lower than the corresponding cyano-acetylene reaction—amplifying the effect of the atom/group with which the radical adds to the acetylene molecule.^{71–73}

6. Conclusion

The reaction of the ¹¹BO radical with acetylene was investigated at a collision energy of 13 kJ mol⁻¹ employing the crossed molecular beam technique and supported by *ab initio* and RRKM calculations. The reaction has no barrier and is initiated by boron addition of the ¹¹BO radical to the π electron density of the acetylene molecule. The reaction indicates indirect scattering dynamics with complex formation, which yields after hydrogen loss, the linear product O¹¹BCCH *via* a tight exit transition state. RRKM calculations suggested that the product was formed *via* two competing channels with a branching ratio of 97 : 3. The major reaction channel resulted in hydrogen loss from the secondary carbon atom of the reaction intermediate O¹¹BHCCH *via* a tight exit transition state located 17 kJ mol⁻¹ above the products. The minor reaction channel resulted in a 1,2-hydrogen shift from the collision complex and subsequent hydrogen loss from the terminal carbon of the reaction intermediate O¹¹BCCH₂ *via* a tight exit transition state located 25 kJ mol⁻¹ above the products. The peaked CM angular distribution is explained by the geometry of the decomposing O¹¹BHCCH complex of the major reaction channel. Here, the four heavy atoms are rotating in the plane almost perpendicular to the total angular momentum vector **J** around the B axis of the complex. According to the microcanonical model of Roger Grice the decomposition of such a transition state leads to a preferential hydrogen loss direction almost parallel to the total angular momentum vector and resulting peaked angular distribution. This study represents the first time a B/O/C/H system has been investigated under single collision conditions and computationally. These data show that ¹¹BOCCH forms in the combustion of boron particles within hydrocarbon based fuels and therefore can be incorporated into the latest combustion models. Furthermore, the dynamics of the reaction between ¹¹BO and acetylene shows marked similarities to the reaction of CN with acetylene, providing information on the BO/CN isoelectronicity. The development of a new boronyl radical molecular beam provides a fertile ground for further investigation into boronyl plus hydrocarbon reactions.

Acknowledgements

This work was supported by the Air Force Office of Scientific Research (A9550-09-1-0177).

References

- 1 A. Osmont, I. Gokalp and L. Catoire, *Propellants, Explos., Pyrotech.*, 2006, **31**, 343–354.
- 2 T. Edwards, *J. Propul. Power*, 2003, **19**, 1089–1107.
- 3 G. W. Burdette, H. R. Lander and J. R. McCoy, *J. Energy*, 1978, **2**, 289–292.
- 4 M. K. King, *Journal of Spacecraft and Rockets*, 1982, **19**, 294.
- 5 C. P. Talley, *Aero/Space Eng.*, 1959, **18**, 37–40,47.
- 6 S. R. Turns, J. T. Holl, A. S. P. Solomon and G. M. Faeth, *Combust. Sci. Technol.*, 1985, **43**, 287–300.
- 7 J. J. Hinchey, *J. Chem. Phys.*, 1993, **99**, 4403–4410.
- 8 M. A. Gurevich, I. M. Kir'yanov and E. S. Ozerov, *Fizika Goreniya i Vzryva*, 1969, **5**, 217–222.
- 9 V. G. Shevchuk, D. I. Polishchuk, A. N. Zolotko, Y. I. Vovchuk and V. B. Osipov, *Fizika Aerodispersnykh Sistem*, 1974, **10**, 69–71.
- 10 Y. I. Vovchuk, A. N. Zolotko, L. A. Klyachko, D. I. Polishchuk and V. G. Shevchuk, *Fizika Goreniya i Vzryva*, 1974, **10**, 615–618.
- 11 Y. I. Vovchuk, A. N. Zolotko, L. A. Kryachko and D. I. Polishchuk, *Fizika Goreniya i Vzryva*, 1975, **11**, 556–563.
- 12 P. Antaki and F. A. Williams, *Combust. Flame*, 1987, **67**, 1–8.
- 13 S. C. Li and F. A. Williams, in *Combustion of Boron-Based Solid Propellants and Solid Fuels*, K. K. Kuo and R. Pein, Begell House/CRC Press, London, 1993, p. 248.
- 14 A. Macek and J. M. Semple, *Combust. Sci. Technol.*, 1969, **1**, 181–191.
- 15 A. Macek and J. M. Semple, *Combustion of boron carbide particles*, Atl. Res. Div., Susquehanna Corp., Alexandria, VA, USA, 1971.
- 16 S. Yuasa, T. Yoshida, M. Kawashima and H. Isoda, *Combust. Flame*, 1998, **113**, 380–387.
- 17 R. C. Brown, C. E. Kolb, S. Y. Cho, R. A. Yetter, F. L. Dryer and H. Rabitz, *Int. J. Chem. Kinet.*, 1994, **26**, 319–332.
- 18 R. C. Brown, C. E. Kolb, R. A. Yetter, F. L. Dryer and H. Rabitz, *Combust. Flame*, 1995, **101**, 221–238.
- 19 W. Zhou, R. A. Yetter, F. L. Dryer, H. Rabitz, R. C. Brown and C. E. Kolb, *Combust. Flame*, 1998, **112**, 507–521.
- 20 W. Zhou, R. A. Yetter, F. L. Dryer, H. Rabitz, R. C. Brown and C. E. Kolb, *Chemical and Physical Processes in Combustion*, 1996, 495–498.
- 21 W. Zhou, R. A. Yetter, F. L. Dryer, H. Rabitz, R. C. Brown and C. E. Kolb, *Combust. Flame*, 1999, **117**, 227–243.
- 22 F. Zhang, X. Gu, R. I. Kaiser and H. Bettinger, *Chem. Phys. Lett.*, 2007, **450**, 178–185.
- 23 L. Andrews, P. Hassanzadeh, J. M. L. Martin and P. R. Taylor, *J. Phys. Chem.*, 1993, **97**, 5839–5847.
- 24 R. I. Kaiser, N. Balucani, N. Galland, F. Caralp, M. T. Rayez and Y. Hannachi, *Phys. Chem. Chem. Phys.*, 2004, **6**, 2205–2210.
- 25 N. Balucani, O. Asvany, Y. T. Lee, R. I. Kaiser, N. Galland and Y. Hannachi, *J. Am. Chem. Soc.*, 2000, **122**, 11234–11235.
- 26 F. Zhang, X. Gu, R. I. Kaiser, N. Balucani, C. H. Huang, C. H. Kao and A. H. H. Chang, *J. Phys. Chem. A*, 2008, **112**, 3837–3845.
- 27 F. Zhang, Y. Guo, X. Gu and R. I. Kaiser, *Chem. Phys. Lett.*, 2007, **440**, 56–63.
- 28 H. F. Bettinger and R. I. Kaiser, *J. Phys. Chem. A*, 2004, **108**, 4576–4586.
- 29 F. Zhang, H. L. Sun, A. H. H. Chang, X. Gu and R. I. Kaiser, *J. Phys. Chem. A*, 2007, **111**, 13305–13310.
- 30 D. Sillars, R. I. Kaiser, N. Galland and Y. Hannachi, *J. Phys. Chem. A*, 2003, **107**, 5149–5156.
- 31 F. Zhang, C. H. Kao, A. H. H. Chang, X. Gu, Y. Guo and R. I. Kaiser, *ChemPhysChem*, 2008, **9**, 95–105.
- 32 N. Balucani, F. Zhang and R. I. Kaiser, *Chem. Rev.*, 2010, **110**, 5107–5127.
- 33 M. K. King, *Combust. Sci. Technol.*, 1972, **5**, 155–164.
- 34 G. Mohan and F. A. Williams, *AIAA J.*, 1972, **108**, 776–783.
- 35 S. C. Li and F. A. Williams, *Symp. (Int.) Combust., [Proc.]*, 1991, **23**, 1147–1154.
- 36 S. C. Li, *Combust. Sci. Technol.*, 1991, **77**, 149–169.
- 37 C. L. Yeh and K. K. Kuo, *Transport Phenomena in Combustion, Proceedings of the International Symposium on Transport Phenomena in Combustion, 8th, San Francisco, July 16–20, 1995*, 1996, **1**, 45–63.
- 38 C. L. Yeh and K. K. Kuo, *Prog. Energy Combust. Sci.*, 1997, **22**, 511–541.
- 39 C. L. Yeh and K. K. Kuo, *Transport Phenomena in Combustion, Proceedings of the International Symposium on Transport Phenomena in Combustion, 8th, San Francisco, July 16–20, 1995*, 1996, **2**, 1461–1472.
- 40 B. Hussmann and M. Pfitzner, *Combust. Flame*, 2010, **157**, 822–833.
- 41 B. Hussmann and M. Pfitzner, *Combust. Flame*, 2010, **157**, 803–821.
- 42 S. H. Bauer, *Chem. Rev.*, 1996, **96**, 1907–1916.

- 43 N. L. Garland, C. T. Stanton, H. H. Nelson and M. Page, *J. Chem. Phys.*, 1991, **95**, 2511–2515.
- 44 M. Page, *Multireference configuration interaction study of the reaction: molecular hydrogen+boron oxide (BO) yields atomic hydrogen+hydrogen boride oxide (HBO)*, Nav. Res. Lab., Washington, DC, USA, 1988.
- 45 C.-H. Chin, A. M. Mebel and D.-Y. Hwang, *J. Phys. Chem. A*, 2004, **108**, 473–483.
- 46 S.-D. Li, J.-C. Guo and G.-M. Ren, *THEOCHEM*, 2007, **821**, 153–159.
- 47 A. Papakondylis and A. Mavridis, *J. Phys. Chem. A*, 2001, **105**, 7106–7110.
- 48 C. Ollivier and P. Renaud, *Chem. Rev.*, 2001, **101**, 3415–3434.
- 49 H.-J. Zhai, S.-D. Li and L.-S. Wang, *J. Am. Chem. Soc.*, 2007, **129**, 9254–9255.
- 50 L. C. L. Huang, O. Asvany, A. H. H. Chang, N. Balucani, S. H. Lin, Y. T. Lee, R. I. Kaiser and Y. Osamura, *J. Chem. Phys.*, 2000, **113**, 8656–8666.
- 51 X. Gu, Y. Guo, F. Zhang, A. M. Mebel and R. I. Kaiser, *Faraday Discuss.*, 2006, **133**, 245–275.
- 52 X. Gu, Y. Guo, E. Kawamura and R. I. Kaiser, *J. Vac. Sci. Technol., A*, 2006, **24**, 505–511.
- 53 X. B. Gu, Y. Guo, E. Kawamura and R. I. Kaiser, *Rev. Sci. Instrum.*, 2005, **76**, 083115.
- 54 Y. Guo, X. Gu, E. Kawamura and R. I. Kaiser, *Rev. Sci. Instrum.*, 2006, **77**, 034701.
- 55 M. Vernon, *Thesis*, University of California, Berkeley, 1981.
- 56 M. S. Weis, *PhD Thesis*, University of California, Berkeley, 1986.
- 57 R. I. Kaiser, P. Paksyutenko, C. Ennis, F. Zhang, X. Gu, S. Krishtal, A. M. Mebel, O. Kostko and A. M., *Faraday Discuss.*, 2010, **147**, 429.
- 58 X. Tan, CyberWit, Santa Clara, 1.4.1.1 edn, 2004.
- 59 F. Melen, I. Dubois and H. Bredohl, *J. Phys. B: At. Mol. Phys.*, 1985, **18**, 2423–2432.
- 60 R. W. Nicholls, P. A. Fraser and W. R. Jarman, *Combust. Flame*, 1959, **3**, 13–38.
- 61 A. D. Becke, *J. Chem. Phys.*, 1993, **98**, 5648–5652.
- 62 C. Lee, W. Yang and R. G. Parr, *Phys. Rev. B*, 1988, **37**, 785–789.
- 63 C. Hampel, K. A. Peterson and H. J. Werner, *Chem. Phys. Lett.*, 1992, **190**, 1–12.
- 64 G. D. Purvis, III and R. J. Bartlett, *J. Chem. Phys.*, 1982, **76**, 1910–1918.
- 65 P. J. Knowles, C. Hampel and H. J. Werner, *J. Chem. Phys.*, 1993, **99**, 5219–5227.
- 66 M. J. O. Deegan and P. J. Knowles, *Chem. Phys. Lett.*, 1994, **227**, 321–326.
- 67 M. J. Frisch, G. W. Trucks, H. B. Schlegel, G. E. Scuseria, M. A. Robb, J. R. Cheeseman, V. G. Zakrzewski, J. A. Montgomery, Jr., R. E. Stratmann, J. C. Burant, S. Dapprich, J. M. Millam, A. D. Daniels, K. N. Kudin, M. C. Strain, O. Farkas, J. Tomasi, V. Barone, M. Cossi, R. Cammi, B. Mennucci, C. Pomelli, C. Adamo, S. Clifford, J. Ochterski, G. A. Petersson, P. Y. Ayala, Q. Cui, K. Morokuma, P. Salvador, J. J. Dannenberg, D. K. Malick, A. D. Rabuck, K. Raghavachari, J. B. Foresman, J. Cioslowski, J. V. Ortiz, A. G. Baboul, B. B. Stefanov, G. Liu, A. Liashenko, P. Piskorz, I. Komaromi, R. Gomperts, R. L. Martin, D. J. Fox, T. Keith, M. A. Al-Laham, C. Y. Peng, A. Nanayakkara, M. Challacombe, P. M. W. Gill, B. G. Johnson, W. Chen, M. W. Wong, J. L. Andres, C. Gonzalez, M. Head-Gordon, E. S. Replogle and J. A. Pople, *GAUSSIAN 98 (Revision A.11)*, Gaussian, Inc., Pittsburgh, PA, 2001.
- 68 A. H. H. Chang, A. M. Mebel, X. M. Yang, S. H. Lin and Y. T. Lee, *J. Chem. Phys.*, 1998, **109**, 2748–2761.
- 69 W. B. Miller, S. A. Safron and D. R. Herschbach, *Discuss. Faraday Soc.*, 1967, **44**, 108–122.
- 70 R. Grice and D. J. Smith, *Mol. Phys.*, 1993, **80**, 1533–1540.
- 71 R. I. Kaiser, F. Stahl, P. v. R. Schleyer and H. F. Schaefer, III, *Phys. Chem. Chem. Phys.*, 2002, **4**, 2950–2958.
- 72 D. Chastaing, P. L. James, I. R. Sims and I. W. M. Smith, *Faraday Discuss.*, 1998, **109**, 165–181.
- 73 I. R. Sims, J.-L. Queffelec, D. Travers, B. R. Rowe, L. B. Herbert, J. Karthaeuser and I. W. M. Smith, *Chem. Phys. Lett.*, 1993, **211**, 461–468.